European Journal of Radiology 96 (2017) 12–20

Contents lists available at ScienceDirect

European Journal of Radiology

journal homepage: www.elsevier.com/locate/ejrad

Research article

Improved clinical workflow for simultaneous whole-body PET/MRI using high-resolution CAIPIRINHA-accelerated MR-based attenuation correction

Martin T. Freitag[a,*], Matthias Fenchel[b], Philipp Bäumer[a], Thorsten Heußer[c], Christopher M. Rank[c], Marc Kachelrieß[c], Daniel Paech[a], Klaus Kopka[d], Sebastian Bickelhaupt[a], Antonia Dimitrakopoulou-Strauss[e], Klaus Maier-Hein[f], Ralf Floca[f], Mark E. Ladd[c,g], Heinz-Peter Schlemmer[a], Florian Maier[c]

[a] Department of Radiology, German Cancer Research Center (DKFZ), Heidelberg, Germany
[b] Siemens Healthcare GmbH, Erlangen, Germany
[c] Department of Medical Physics in Radiology, German Cancer Research Center (DKFZ), Heidelberg, Germany
[d] Division of Radiopharmaceutical Chemistry, German Cancer Research Center (DKFZ), Heidelberg, Germany
[e] Clinical Cooperation Unit Nuclear Medicine, German Cancer Research Center (DKFZ), Heidelberg, Germany
[f] Junior Group Medical Image Computing, German Cancer Research Center (DKFZ), Heidelberg, Germany
[g] Faculty of Physics and Astronomy and Faculty of Medicine, University of Heidelberg, Heidelberg, Germany

ARTICLE INFO

Keywords:
PET/MRI
Attenuation correction
CAIPIRINHA
Parallel imaging

ABSTRACT

Purpose: To explore the value and reproducibility of a novel magnetic resonance based attenuation correction (MRAC) using a CAIPIRINHA-accelerated T1-weighted Dixon 3D-VIBE sequence for whole-body PET/MRI compared to the clinical standard.

Methods: The PET raw data of 19 patients from clinical routine were reconstructed with standard MRAC ($MRAC_{std}$) and the novel MRAC ($MRAC_{caipi}$), a prototype CAIPIRINHA accelerated Dixon 3D-VIBE sequence, both acquired in 19 s/bed position. Volume of interests (VOIs) for liver, lung and all voxels of the total image stack were created to calculate standardized uptake values (SUV_{mean}) followed by inter-method agreement (Passing-Bablok regression, Bland-Altman analysis). A voxel-wise SUV comparison per patient was performed for intra-individual correlation between $MRAC_{std}$ and $MRAC_{caipi}$. Difference images ($MRAC_{std}$-$MRAC_{caipi}$) of attenuation maps and SUV images were calculated. The image quality of in/opposed-phase water and fat images obtained from $MRAC_{caipi}$ was assessed by two readers on a 5-point Likert-scale including intra-class coefficients for inter-reader agreement.

Results: SUV_{mean} correlations of VOIs demonstrated high linearity ($0.95 < \text{Spearman's rho} < 1$, $p < 0.0001$, respectively), substantiated by voxel-wise SUV scatter-plots (1.79×10^8 pixels). Outliers could be explained by different physiological conditions between the scans such as different segmentation of air-containing tissue, lungs, kidneys, metal implants, diaphragm edge or small air bubbles in the gastrointestinal tracts that moved between MRAC acquisitions. Nasal sinuses and the trachea were better segmented in $MRAC_{caipi}$. High-resolution T1w Dixon 3D VIBE images were acquired in all cases and could be used for PET/MRI fusion. $MRAC_{caipi}$ images were of high diagnostic quality (4.2 ± 0.8) with 0.92-0.96 intra-class correlation.

Conclusions: The novel prototype $MRAC_{caipi}$ extends the value for attenuation correction by providing a high spatial resolution DIXON-based dataset suited for diagnostic assessment towards time-efficient whole-body PET/MRI.

1. Introduction

The fully integrated combination of positron emission tomography (PET) and magnetic resonance imaging (MRI), simultaneous PET/MRI, facilitates the fusion of molecular information provided by PET with high soft tissue contrast, numerous functional imaging methods and reduced radiation exposure by MRI compared to PET/CT [1]. For accurate quantitative PET-imaging, attenuation correction (AC) is the

Abbreviations: AC, attenuation correction; MRI, magnetic resonance imaging; PET, positron emission tomography; VOI, volume of interest; VOI_{liver}, VOI in liver; VOI_{total}, VOI of total image stack; SUV, standardized uptake value; μmap, MR-based attenuation map

* Corresponding author.
E-mail address: m.freitag@dkfz.de (M.T. Freitag).

http://dx.doi.org/10.1016/j.ejrad.2017.09.007
Received 29 April 2017; Received in revised form 17 August 2017; Accepted 12 September 2017

Table 1
Patient demographics included in the quantitative analysis. The thorax was completely included in 9 patients, of which 4 received a whole-body examination.

	age	gender	MBq	height	weight	diagnosis	bed positions	tracer
1	48	m	114	177	81	NET (pancreas)	Thorax-pelvis (3BED)	^{68}Ga-DOTATOC
2	30	f	113	160	46	NET (appendix)	Abdomen (2BED)	^{68}Ga-DOTATOC
3	62	m	121	187	108	PCA	Abdomen (2BED)	^{68}Ga-PSMA-HBED-CC
4	59	m	141	175	63	PCA	Abdomen (2BED)	^{68}Ga-PSMA-HBED-CC
5	74	m	144	182	86	PCA	Thorax-pelvis (3BED)	^{68}Ga-PSMA-HBED-CC
6	66	m	115	178	88	PCA	Head-pelvis (5BED)	^{68}Ga-PSMA-HBED-CC
7	76	m	105	173	87	PCA	Thorax-pelvis (3BED)	^{68}Ga-PSMA-HBED-CC
8	68	m	259	170	70	PCA	Thorax-pelvis (3BED)	^{68}Ga-PSMA-HBED-CC
9	53	m	214	183	80	PCA	Thorax-pelvis (3BED)	^{68}Ga-PSMA-HBED-CC
10	64	m	71	180	80	PCA	Thorax-pelvis (3BED)	^{68}Ga-PSMA-HBED-CC
11	46	m	232	189	83	NHL	Head-pelvis (5BED)	^{18}F-FDG
12	74	m	282	177	76	PCA	Thorax-pelvis (3BED)	^{68}Ga-PSMA-HBED-CC
13	56	m	243	176	95	PCA	Thorax-pelvis (3BED)	^{68}Ga-PSMA-HBED-CC
14	49	m	227	180	80	PCA	Thorax-pelvis (3BED)	^{68}Ga-PSMA-HBED-CC
15	66	m	247	170	68	PCA	Thorax-pelvis (3BED)	^{68}Ga-PSMA-HBED-CC
16	61	m	158	178	82	PCA	Thorax-pelvis (3BED)	^{68}Ga-PSMA-HBED-CC
17	66	m	250	180	80	PCA	Head-pelvis (5BED)	^{68}Ga-PSMA-HBED-CC
18	71	f	371	164	55	BC	Head-pelvis (5BED)	^{18}F-FDG
19	70	m	238	170	75	PCA	Thorax-pelvis (3BED)	^{68}Ga-PSMA-HBED-CC

MBq: injected activity in megabecquerel; NET: neuroendocrine tumor; PCA: prostate carcinoma; BC: bronchial carcinoma; NHL: Non-Hodgkin-Lymphoma

Table 2
Comparison of most relevant sequence parameters of $MRAC_{std}$ versus $MRAC_{caipi}$. CAIPIRINHA-acceleration settings are given in methods.

Parameter	TE1/TE2/TR (ms)	Resolution (mm^3)	Acquisition Time (s)	FOV (mm^2)	Matrix
$MRAC_{std}$	1.23/2.46/3.6	4.1 × 2.6 × 3.1	19	500 × 328	192 × 126
$MRAC_{caipi}$	1.24/2.47/4.26	1.9 × 1.4 × 3.2	19	500 × 500	264 × 352

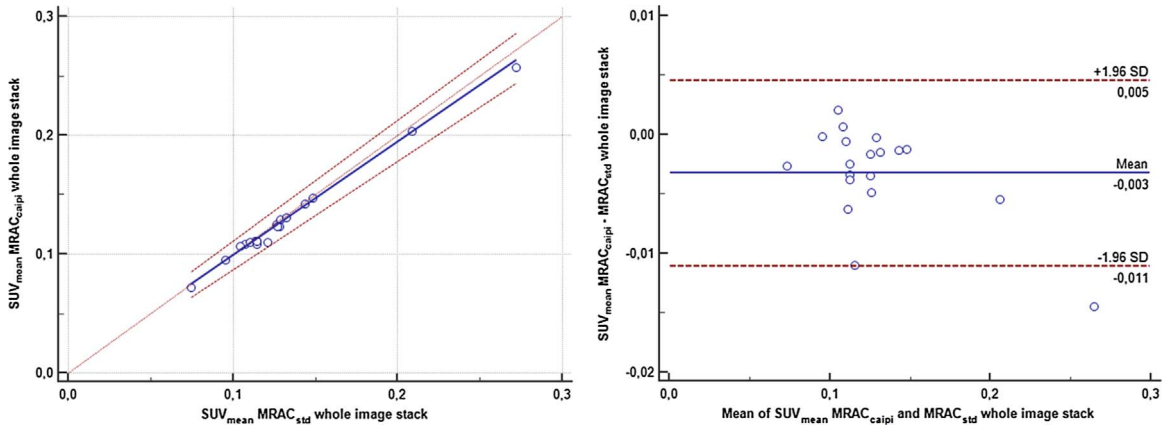

Fig. 1. Passing-Bablok regression (left column) and Bland-Altman plot (right column) for inter-method correlation between VOIs of the whole image stack for SUV_{mean}. Refer to Fig. 1 (Supplementary) for voxel-wise SUV comparison. A high linearity for each plot is demonstrated indicating strong agreement between both methods. $MRAC_{std}$ is plotted on the x-axis, $MRAC_{caipi}$ on the y-axis.

clinical standard to correct for tissue-dependent differences in photon attenuation. In the case of PET/CT, an axial CT scan provides robust attenuation coefficients reflecting tissue density per voxel after conversion to the 511 keV energy of the PET photons [2]. To reduce radiation exposure, a low-dose scan between 30 and 80 mAs is sufficient. However, the downside of this method is the poorer contrast of the low-dose CT scan compared to a normal-dose contrast-enhanced CT scan. Hence, low-dose CT has intrinsic limitations for depicting the anatomy clearly due to low soft tissue contrast, i.e. to correlate a PET-positive finding with the underlying tissue and to differentiate it from adjacent structures such as vessels. In contrast, MRI potentially allows for better correlation images of the underlying anatomy ('landmarking') in areas where high soft tissue contrast is demanded such as brain, head/neck, abdomen and extremities. In contrast to PET/CT, the attenuation map for PET data using MRI is based on automatic tissue classification and assignment of attenuation values for each tissue type [3]. MRAC using T1-weighted Dixon 3D-VIBE-images ($MRAC_{std}$) is a valid approximation and produces reliable results compared to CT-based AC in clinical routine for ^{18}F-FDG, based on previous work including data on more than 2300 patients [4–6]. $MRAC_{std}$ features a comparable poor spatial resolution if re-formatted to axial orientation. However, it can be acquired in only 19 s per bed position. The *generalized autocalibrating partially parallel acquisition* (GRAPPA) algorithm yields an accelerated acquisition of MRI images [7] by acquiring fewer k-space lines. The method then compensates for the undersampled k-space data by exploiting the redundant information of different receiver coil channels. GRAPPA can be extended using *controlled aliasing in parallel imaging results in higher acceleration* (CAIPIRINHA) to improve the parallel imaging results by exploiting the coil sensitivity patterns more efficiently and, thus, allow for larger acceleration factors [8,9]. This technique facilitates high-resolution images for breath-hold examinations [10] in short acquisition times. However, in the case of PET/MRI,